Journal of Power Sources 261 (2014) 184–187

Contents lists available at ScienceDirect

Journal of Power Sources

journal homepage: www.elsevier.com/locate/jpowsour

Short communication

Polymer-pyrolysis assisted synthesis of vanadium trioxide and carbon nanocomposites as high performance anode materials for lithium-ion batteries

Yucheng Dong [a,b,*], Ruguang Ma [c], Mingjun Hu [b], Hua Cheng [b], Jong-Min Lee [c], Yang Yang Li [b], Juan Antonio Zapien [a,b,*]

[a] Center of Super-Diamond and Advanced Films (COSDAF), City University of Hong Kong, Hong Kong, China
[b] Department of Physics and Materials Science, City University of Hong Kong, 83 Tat Chee Avenue, Kowloon, Hong Kong, China
[c] School of Chemical and Biomedical Engineering, Nanyang Technological University, Singapore 637459, Singapore

HIGHLIGHTS

- Vanadium trioxide and carbon nanocomposites were synthesized by a simple polymer-pyrolysis assisted method.
- The metal complex atomistically distributed throughout the viscous polymer structure.
- The as-prepared vanadium trioxide and carbon nanocomposites electrode possesses superior battery performance.

ARTICLE INFO

Article history:
Received 18 January 2014
Received in revised form
20 February 2014
Accepted 6 March 2014
Available online 16 March 2014

Keywords:
Lithium-ion batteries
Vanadium trioxide
Polymer-pyrolysis
Carbon nanocomposites

ABSTRACT

We present a simple polymer-pyrolysis assisted method to prepare vanadium trioxide and carbon nanocomposites as an advanced anode material for lithium-ion batteries. The as-prepared material deliver a superior battery performance with highly retained capacity of ~780 mAh g^{-1} over 100 cycles at a current density of 200 mA g^{-1}, showing excellent cyclic stability, and good rate capability. The improved electrochemical performance of vanadium trioxide and carbon nanocomposites electrode makes it promising as a suitable anode material for practical battery applications.

1. Introduction

In the past decade, rechargeable lithium-ion batteries (LIBs) have been extensively used as power sources for electronic devices [1]. Afterward, an increasing attention was diverted to explore suitable power supplies for electrical/hybrid vehicles thus greatly increasing market demand for materials with high specific capacity, durable cyclic stability, good rate capability and cost-effective to replace the commercially successful graphitic anode (372 mAh g^{-1}). As a result, intense research aims to explore new electrode materials with enhanced electrochemical performance for LIBs. Transition-metal oxides, such as Fe_3O_4, Co_3O_4 and MoO_3, have been widely investigated as potential anode materials for LIBs due to their high theoretical capacity [2–4]. Among them, vanadium trioxide (V_2O_3) has been identified as a viable candidate for LIBs because of its high theoretical capacity (1070 mAh g^{-1}), low toxicity and natural abundance [5]. However, progress on the application of V_2O_3 as anode material in LIBs lags behind other transition-metal oxides due to its perceived disadvantage resulting from its poor conductivity [6]. Therefore, to improve the conductivity of V_2O_3, conductive carbon has to be incorporated into the system, which also serves as cushion layer to accommodate the volume change during the cycle processes.

Herein, we report a polymer-pyrolysis assisted route to prepare vanadium trioxide and carbon nanocomposites (V_2O_3/C NCs). Compared with carbon free V_2O_3 nanoparticles (C-free V_2O_3 NPs)

* Corresponding authors. Center of Super-Diamond and Advanced Films (COSDAF), City University of Hong Kong, Hong Kong, China.
E-mail addresses: yc-d@hotmail.com (Y. Dong), apjazs@cityu.edu.hk (J.A. Zapien).

http://dx.doi.org/10.1016/j.jpowsour.2014.03.020
0378-7753/

electrode prepared under the same experimental conditions, the as-prepared V_2O_3/C NCs electrode possesses much better electrochemical performance, such as high specific capacity, excellent cyclic stability, and good rate capability.

2. Experimental

The V_2O_3/C NCs were synthesized by a simple polymer-pyrolysis assisted method as follows. First, 0.81 g oxalic acid ($H_2C_2O_4$) and 0.54 g commercial vanadium pentoxide (V_2O_5) were dissolved in 5 mL distilled water under stirring at room temperature until the color of the solution changed from yellow to blue [7]. Then, 0.25 g glucose ($C_6H_{12}O_6$) and 0.45 g polyethylene oxide (PEO, Relative molecular mass: 500000) were successively added to the above solution under active stirring at 60 °C until a homogeneous viscous liquid was obtained. The general idea is to distribute the metal complex atomistically throughout the viscous polymer structure so that the precursor solution generates in situ a polar mesoporous carbonaceous material during the evaporation process [8]. Next, the resulting viscous liquid was dried at 80 °C for 24 h to complete dehydration and form a well-distributed polyacrylate. Finally, the obtained copolymeric product was annealed at 600 °C for 3 h under argon atmosphere.

Phases of the products were characterized by micro-area X-ray diffraction (XRD, Philips X'Pert MRD). Raman spectroscopy (Renishaw 2000, Raman microscope with 633 nm argon ion laser) was employed to verify chemical bonding characteristics of V_2O_3 and carbon. The morphological characteristics of V_2O_3/C NCs were investigated by scanning electron microscopy (SEM, Philips, XL 30FEG). The electrochemical measurements were performed using coin cells (2032) with lithium foil as counter electrode. The working electrodes were prepared by mixing the active material (V_2O_3/C NCs), acetylene carbon black and polyvinylidene fluoride (PVDF) with a weight ratio of 80:10:10 dissolved in 1-methyl-2-pyrrolidinone (NMP) to form a slurry which was uniformly coated on copper foil and dried at 100 °C for 8 h in a vacuum oven. Celgard 2032 (Celgard, Inc., USA) served as the separator and a solution of 1 M $LiPF_6$ in ethylene carbonate/dimethyl carbonate (EC:DEC = 1:1, v/v) as the electrolyte.

Cyclic voltammograms (CV) were obtained on a CHI-660C electrochemical workstation, on which electrochemical impedance spectroscopy (EIS) measurements were also conducted in a frequency range from 10 mHz to 100 kHz with a potentiostatic signal amplitude of 5 mV. Galvanostatic discharge/charge cycling measurement was performed on an Arbin Instruments (BT 2000, College Station, Texas, USA) battery test system at various C rates (1C = 1000 mA g^{-1}) between 5 mV and 3 V versus Li^+/Li at room temperature. Note that the mass of carbon was included when calculating the capacity of V_2O_3/C NCs.

3. Results and discussion

Fig. 1(a) shows the morphology of the V_2O_3/C NCs. The voids can be observed between particles, which were produced by CO and CO_2 release when the precursor decomposed during annealing process [7]. It has been suggested that the voids enable rapid electrolyte transport and consequently more efficient ion diffusion and better energy storage [9]. The crystalline structure of the V_2O_3/

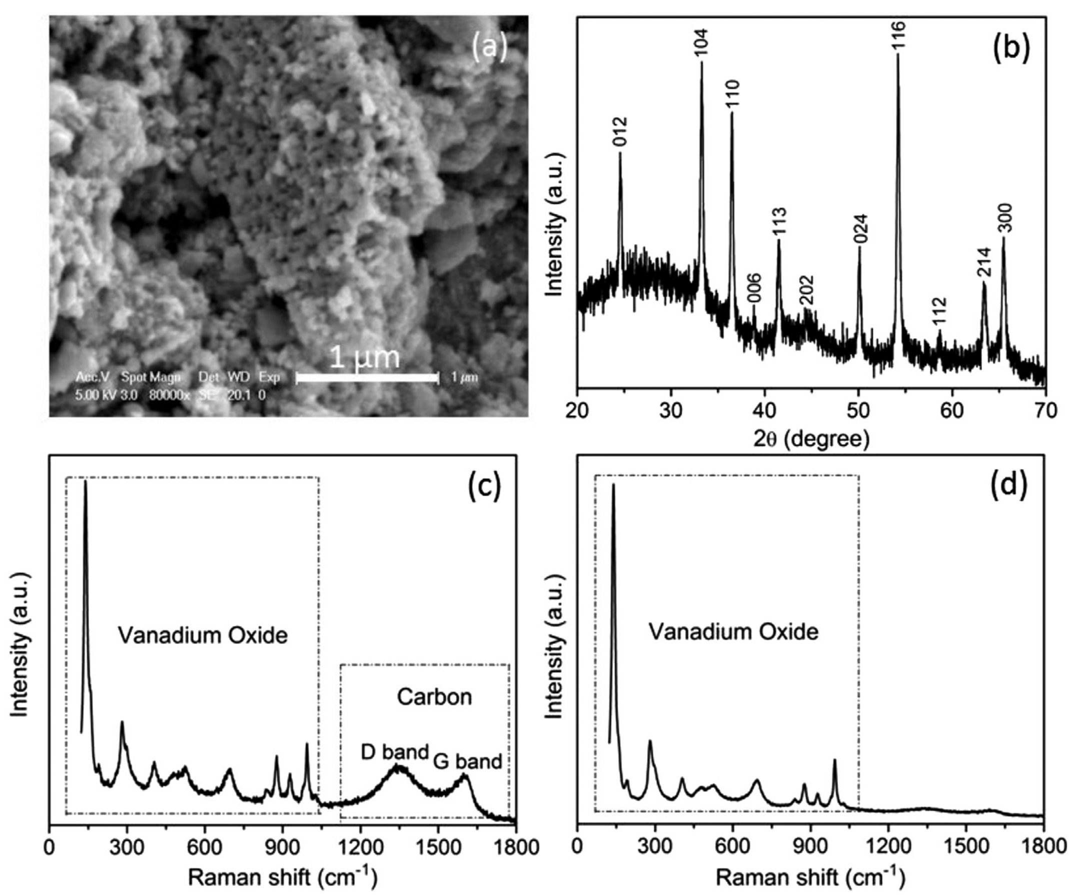

Fig. 1. (a) SEM image and (b) XRD pattern of V_2O_3/C NCs; Raman spectra of (c) C-free V_2O_3 NPs and (d) V_2O_3/C NCs.

C NCs was examined by XRD. A representative spectrum, Fig. 1(b), shows that all the diffraction peaks and relative intensities of V_2O_3 are consistent with those of V_2O_3 (PDF 001-1293), confirming the good crystallinity of the product. The conspicuous and broad peaks at $\sim 26°$ and $\sim 44°$ are attributed to disordered carbon generated from thermal decomposition of glucose [10]. This is further confirmed by Raman spectroscopy as shown in Fig. 1(c), which clearly shows the existence of carbon and vanadium oxide in the composites. The Raman spectrum of V_2O_3 has been scarcely reported due to its poor light scattering, especially in the presence of carbon composites [11]. The peaks displayed below 1000 cm^{-1} correspond to the characteristic features of crystalline vanadium oxide as reported previously [6,12]. In addition, two broad peaks at ~ 1340 cm^{-1} and ~ 1600 cm^{-1} corresponding to the D and G bands of disordered/graphitic carbon [13], respectively, are clearly observed in the spectrum of Fig. 1(c). Compared to the G band, the stronger intensity of the D band indicates the disordered amorphous nature of the carbon in the composites. The Raman spectrum of C-free V_2O_3 NPs is also shown in Fig. 1(d) which possesses similar peaks below 1000 cm^{-1} with those of V_2O_3/C NCs.

The electrochemical performance of the V_2O_3/C NCs is shown in Fig. 2. The CV analysis was applied to investigate the electrochemical details between 5 mV and 3 V at a scan rate of 0.1 mV s^{-1} for the first three cycles as shown in Fig. 2(a). Two peaks clearly appeared at voltage potentials of ~ 0.72 and ~ 1.38 V in the first cathodic cycle and disappeared in the subsequent cycles, which could be attributed to an irreversible reaction related to electrolyte decomposition and formation of a solid electrolyte interface (SEI) layer [14]. In the anodic scan, a broad peak related to the oxidation reaction at ~ 2.05 V was recorded. Furthermore, there is no noticeable change of peak intensity and integrated areas for both cathodic and anodic peaks after the first cycle, thus suggesting the good electrochemical reversibility of the V_2O_3/C NCs electrode. Fig. 2(b) shows the galvanostatic discharge/charge profile of the V_2O_3/C NCs electrode at the rate of 0.1 C between 0.05 and 3 V (versus Li^+/Li) for the first five cycles. The initial discharge and charge capacities of the V_2O_3/C NCs electrode were as high as 1441 and 969 mAh g^{-1} with a Coulombic efficiency of 67.2%. The electrochemical conversion reaction mechanism of Li and V_2O_3 can be described as follows:

$$V_2O_3 + xLi^+ + xe \leftrightarrow Li_xV_2O_3 \quad (1)$$

$$Li_xV_2O_3 + (6-x)Li^+ + (6-x)e \leftrightarrow 2V + 3Li_2O \quad (2)$$

During discharge, lithium ions are firstly inserted into V_2O_3 to form $Li_xV_2O_3$ as shown in Eq. (1) [15,16]. While more Li^+ ion are inserted with the decrease of potential, $Li_xV_2O_3$ were totally reduced to metallic vanadium accompanying the formation of Li_2O, as shown in Eq. (2) [6]. During the charge process, the reverse reactions occur. However, it is difficult to drive the reverse reactions to proceed completely to the same extent as the starting materials of forward reactions due to over potential [17,18]. This is why the initial Coulombic efficiency is a little low. The absence of remarkable flat potential plateaus on the discharge/charge curves could be ascribed to several smoothly transition species originating from the multivalence of vanadium [6,19]. The relationship that the valence state decreases with decreasing potential was also reported for other transition-metal oxides [20–22]. The initial discharge capacity is higher than theoretical capacity of V_2O_3; similar phenomena has been usually reported for transition-metal oxides anode and is usually attributed to the formation of a pseudo-

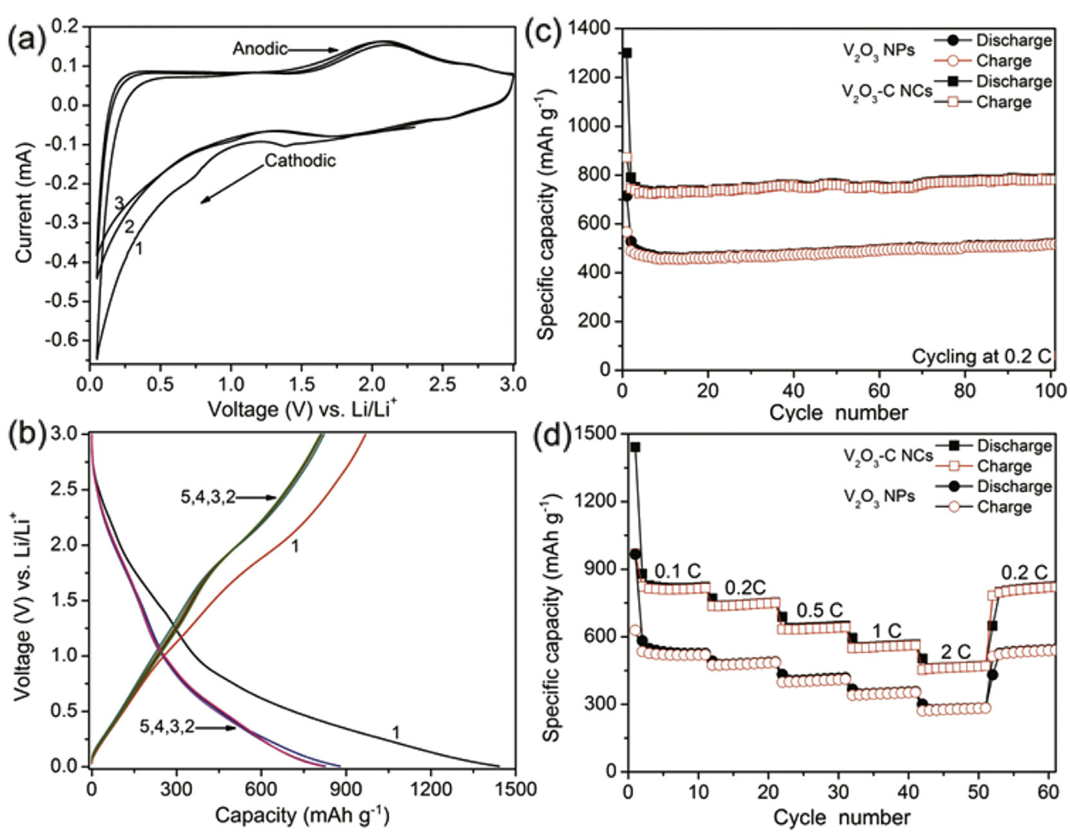

Fig. 2. (a) Cyclic voltammograms and (b) galvanostatic discharge/charge profile of the V_2O_3/C NCs electrode; (c) cyclic performance and (d) rate capability of C-free V_2O_3 NPs and V_2O_3/C NCs electrodes, respectively.

capacitive gel like film resulting from the electrolyte decomposition at low voltages that cause the high irreversible capacity [23]. The capacity of the V_2O_3/C NCs electrode remains almost unchanged through the subsequent four cycles while the Coulombic efficiency exceeds 99% on the fifth cycle, which can be ascribed to the efficiently synergetic effect between V_2O_3 and carbon.

Fig, 2(c) shows the comparison of cyclic performance between the V_2O_3/C NCs and C-free V_2O_3 NPs electrodes at a constant current rate of 0.2 C. As expected, the V_2O_3/C NCs electrode demonstrates a better cyclic retention. A high reversible capacity remains ~730 mAh g^{-1} over 10 cycles, then gradually increases to ~780 mAh g^{-1} after 100 cycles. In contrast, the V_2O_3 NPs electrode initially exhibits a lower capacity of ~460 mAh g^{-1} over 10 cycles, then its capacity increases to ~520 mAh g^{-1} after 100 cycles. This behavior effectively proves the positive impact of carbon incorporation in the composites. The capacity rise after prolonged cycling has been observed for other anode materials and has been attributed to a possible activation process, in which the irreversible Li_2O formed during early cycles could be re-exposed due to progressive pulverization resulting from electrochemical grinding effects [24,25]. To further evaluate the rate capability of the electrodes, new cells were assembled and cycled by increasing the current rates from 0.1 to 2 C as shown in Fig. 2(d). Obviously, the V_2O_3/C NCs electrode exhibits higher reversible capacities than the V_2O_3 NPs electrode at all measured current rates. Furthermore, a stable capacity ~780 mAh g^{-1} was recovered when returning the current rate to 0.2 C and a slight capacity increase was observed for another 10 cycles, demonstrating the excellent reversibility of the V_2O_3/C NCs electrode.

EIS further illustrates the merits of the V_2O_3/C NCs electrode compared to the C-free V_2O_3 NPs electrode. The Nyquist plots (Z′ vs. −Z″) for the assembled electrodes in the frequency range from 100 kHz to 10 mHz are shown in Fig. 3. The high-frequency semicircle can be attributed to the formation of a passivation layer (SEI) which creates a corresponding impedance at the surface of the working electrode in contact with the electrolyte [26]. The semicircle at intermediate frequency describes the charge transfer impedance (R_{ct}) through the electrode/electrolyte interface, which is considered a large proportion of the overall cell's kinetic impedance [27]. The sloping line at low frequency region known as Warburg impedance, represents the Li^+ ion diffusion/transport in the electrolyte to the electrode's surface [28]. It is obvious that the size of the semicircle for V_2O_3/C NCs electrode is smaller than that of C-free V_2O_3 NPs electrode, indicating the enhanced charge transfer at the electrode/electrolyte interface. In the low frequency region, the smaller slope of the V_2O_3/C NCs compared to the C-free V_2O_3 NPs, is a further evidence of the faster Li^+ ion diffusion/transport behavior of the V_2O_3/C NCs electrode. These results are consistent with an increased contact area and clearly demonstrate the enhanced electrical conductivity of the V_2O_3/C NCs electrode. The enhanced electrical conductivity and faster Li^+ ion diffusion/transport in the V_2O_3/C NCs electrode due to the incorporation of carbon in the composites.

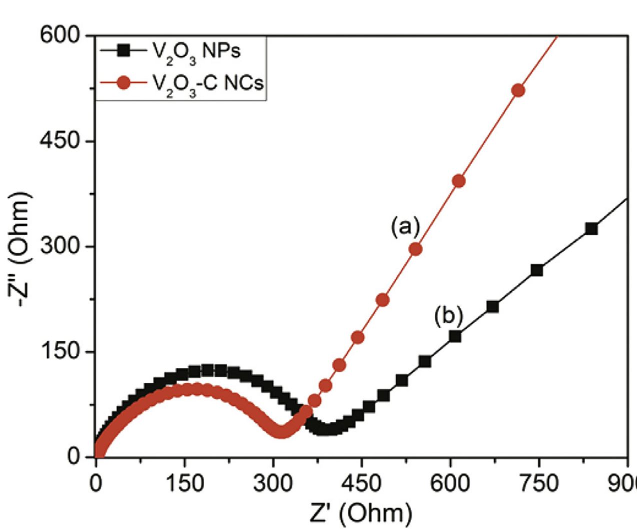

Fig. 3. Nyquist plots (Z′ vs. −Z″) of (a) V_2O_3/C NCs and (b) C-free V_2O_3 NPs electrodes.

4. Conclusion

In summary, V_2O_3/C NCs have been successfully prepared through the thermolysis of a polymer matrix-based metal precursor solution. The V_2O_3/C NCs electrode presented outstanding electrochemical performance due to the synergetic effect between V_2O_3 and carbon in the composites. The assembled electrode could deliver a high capacity of ~780 mAh g^{-1} up to 100 cycles at a current density of 200 mA g^{-1} with excellent cyclic stability, and good rate capability. Accordingly, the polymer-pyrolysis assisted V_2O_3/C NCs are considered as a potential anode material for LIBs.

Acknowledgment

This work was fully supported by a grant from the Research Grants Council of the Hong Kong Special Administrative Region, China (Project No. CityU 122812).

References

[1] M.S. Whittingham, Chem. Rev. 104 (2004) 4271.
[2] N.Q. Zhao, S. Wu, C.N. He, Z.Y. Wang, C.S. Shi, E.Z. Liu, J.J. Li, Carbon 57 (2013) 130.
[3] S.B. Yang, X.L. Feng, S. Ivanovici, K. Müllen, Angew. Chem. Int. Ed. 49 (2010) 8408.
[4] H. Srirama, S. Kuppan, B. Palani, Electrochem. Commun. 31 (2013) 5.
[5] H. Li, P. Balaya, J. Maier, J. Electrochem. Soc. 151 (2004) A1878.
[6] Y. Wang, H.J. Zhang, A.S. Admar, J.Z. Luo, C.C. Wong, A. Borgna, J.Y. Lin, RSC Adv. 2 (2012) 5748.
[7] A.Q. Pan, J.G. Zhang, Z.M. Nie, G.Z. Cao, B.W. Arey, G.S. Li, S.Q. Liang, J. Liu, J. Mater. Chem. 20 (2010) 9193.
[8] P. Pramanik, Bull. Mater. Sci. 22 (1999) 335.
[9] B. Saravanakumar, K.K. Purushothaman, G. Muralidharan, ACS Appl. Mater. Interfaces 4 (2012) 4484.
[10] G. Sandi, R.E. Winans, K.A. Carrado, J. Phys. Chem. C 143 (1996) L95.
[11] C. Piccirillo, R. Binions, I.P. Parkin, Chem. Vap. Depos. 13 (2007) 145.
[12] V.G. Pol, S.V. Pol, J.M. Calderon-Moreno, A. Gedanken, J. Phys. Chem. C 113 (2009) 10500.
[13] F. Tuinstra, J. Koenig, J. Chem. Phys. 53 (1970) 1126.
[14] J. Yao, X.P. Shen, B. Wang, H.K. Liu, G.X. Wang, Electrochem. Commun. 11 (2009) 1849.
[15] Y.F. Sun, S.S. Jiang, W.T. Bi, C.Z. Wu, Y. Xie, J. Power Sources 196 (2011) 8644.
[16] Y.F. Zhang, M.J. Fan, X.H. Liu, C. Huang, H.B. Li, Eur. J. Inorg. Chem. 2012 (2012) 1650.
[17] R.G. Ma, Y.C. Dong, L.J. Xi, S.L. Yang, Z.G. Lu, C.Y. Chung, ACS Appl. Mater. Interfaces 5 (2013) P892.
[18] J.B. Goodenough, K.S. Park, J. Am. Chem. Soc. 135 (2013) P1167.
[19] L.X. Zeng, C. Zheng, J.C. Xi, H.L. Fei, M.D. Wei, Carbon 62 (2013) 382.
[20] Y. Wang, H.J. Zhang, W.X. Lim, J.Y. Lin, C.C. Wong, J. Mater. Chem. 21 (2011) 2362.
[21] L.X. Zeng, F.Y. Xiao, J.C. Wang, S.K. Gao, X.K. Ding, M.D. Wei, J. Mater. Chem. 22 (2012) 14284.
[22] S.B. Yang, Y.J. Gong, Z. Liu, L. Zhan, D.P. Hashim, L.L. Ma, R. Vajtai, P.M. Ajayan, Nano Lett. 13 (2013) 1596.
[23] N.A. Kaskhedikar, J. Maier, Adv. Mater. 21 (2009) 2664.
[24] Y.C. Dong, R.G. Ma, M.J. Hu, H. Cheng, Q.D. Yang, Y.Y. Li, J.A. Zapien, Phys. Chem. Chem. Phys. 15 (2013) 7174.
[25] T. Zhu, J.S. Chen, X.W. Lou, J. Phys. Chem. C 115 (2011) 9814.
[26] D. Aurbach, J. Power Sources 89 (2000) 206.
[27] S.A. Needham, G.X. Wang, K. Konstantinov, Y. Tournayre, Z. Lao, H.K. Liu, Electrochem. Solid State Lett. 9 (2006) A315.
[28] A.D. Fabio, A. Giorgi, M. Mastragostino, F. Soavi, J. Electrochem. Soc. 148 (2001) A845.